



THE UNIVERSITY *of* EDINBURGH

Edinburgh Research Explorer

## Droplet Motion on Contrasting Striated Surfaces

**Citation for published version:**

Zhao, H, Orejon Mantecon, D, Mackenzie-Dover, C, Valluri, P, Shanahan, MER & Sefiane, K 2020, 'Droplet Motion on Contrasting Striated Surfaces', *Applied Physics Letters*, vol. 116, 251604.  
<https://doi.org/10.1063/5.0009364>

**Digital Object Identifier (DOI):**

[10.1063/5.0009364](https://doi.org/10.1063/5.0009364)

**Link:**

[Link to publication record in Edinburgh Research Explorer](#)

**Document Version:**

Peer reviewed version

**Published In:**

Applied Physics Letters

**General rights**

Copyright for the publications made accessible via the Edinburgh Research Explorer is retained by the author(s) and / or other copyright owners and it is a condition of accessing these publications that users recognise and abide by the legal requirements associated with these rights.

**Take down policy**

The University of Edinburgh has made every reasonable effort to ensure that Edinburgh Research Explorer content complies with UK legislation. If you believe that the public display of this file breaches copyright please contact [openaccess@ed.ac.uk](mailto:openaccess@ed.ac.uk) providing details, and we will remove access to the work immediately and investigate your claim.



# Droplet Motion on Contrasting Striated Surfaces

Hongyu Zhao<sup>a</sup>, Daniel Orejon<sup>a</sup>, Coinneach Mackenzie-Dover<sup>b</sup>, Prashant Valluri<sup>a</sup>, Martin E.R.

Shanahan<sup>c</sup> and Khellil Sefiane<sup>a,d\*</sup>

<sup>a</sup>Institute for Multiscale Thermofluids, School of Engineering, The University of Edinburgh, King's Building's,  
Mayfield Road, Edinburgh EH9 3FD, United Kingdom;

<sup>b</sup>Oden Institute for Computational Engineering and Sciences, The University of Texas at Austin, Texas TX  
78712, USA;

<sup>c</sup>University of Bordeaux, I2M, CNRS UMR 5295, F-33400 Talence, France

<sup>d</sup>Tianjin Key Lab of Refrigeration Technology, Tianjin University of Commerce, Tianjin City 300134, China

## Abstract

Liquid droplets move readily under the influence of surface tension gradients on their substrates. Substrates decorated with parallel microgrooves, or striations, presenting the advantage of homogeneous chemical properties yet varying the topological characteristics on either side of a straight-line boundary are considered in this study. The basic type of geometry consists of hydrophobic micro-striations/rails perpendicular to the boundary, with the systematic variation of the width to spacing ratio, thus changing the solid-liquid contact fraction and inducing a well-defined wettability contrast across the boundary. Droplets in the Cassie-Baxter state, straddling the boundary, move along the wettability contrast in order to reduce the overall surface free energy. Results show the importance of average solid fraction and contrasting fraction in a wide range for given geometries across the boundary on droplet motion. A unified criterion for contrasting striated surfaces, which describes the displacement and the velocity of the droplets, is suggested, providing guidelines for droplet manipulation on micro-striated/railed surfaces.

\*Corresponding Author: Khellil Sefiane. Email address: k.sefiane@ed.ac.uk.

Droplet manipulation has attracted increasing interest over the last few years and is rich in potential applications in many industrial and everyday life such as self-cleaning,<sup>1</sup> anti-icing,<sup>2</sup> dropwise condensation heat transfer<sup>3,4</sup> and water harvest.<sup>5</sup> Besides, compared with bulk liquid, microscale droplet-based devices not only require a much lower cost to operate but also facilitate a large number of individual experiments to be undertaken under special conditions simultaneously. These features are of great importance to the optimization of chemical analysis and bioassay systems, where the motion of droplets needs to be controlled precisely.<sup>6-9</sup>

Microscale droplet motion can be instigated by tuning the properties of the surface tension of the droplet or the surface on which the droplet is transported. This is because surface tension dominates the behaviour of the droplet for droplet sizes below the capillary length  $\kappa^{-1}$  ( $\kappa^{-1} = \sqrt{\gamma/\Delta\rho g}$  where  $\gamma, \Delta\rho, g$  are the liquid-gas surface tension, density difference between liquid

and gas phases and gravitational acceleration respectively;  $\kappa^{-1}$  is ca. 2.7 mm for water in air). By tuning the properties of the solid surface and/or those of the liquid droplet, motion of the droplet can be activated by several different methods. The seminal work of Chaudhury and Whitesides reported the motion of a droplet uphill on a surface tilted at  $15^\circ$  in the presence of a spatial chemical wettability gradient from hydrophobic to hydrophilic on a flat smooth surface.<sup>10</sup> Following their work, chemical gradients were used to tune the wettability and thus to induce various kinds of droplet motion.<sup>11-15</sup> Besides, since surface tension is temperature-dependent, droplets deposited on a surface under a temperature gradient moved from hot to cold regions in the work of Brozka *et al.*<sup>16</sup> Droplet motion has also been activated by means of light,<sup>17</sup> electrowetting<sup>18</sup> and the above-mentioned combinations of methods.<sup>19</sup> However, these latter methods rely on the application of applied external forces.

Previous work has demonstrated that surface structure and, more specifically, surface microstructure can also be exploited to finely tune the surface wettability, thus creating an alternative method to activate droplet motion.<sup>20-26</sup> Compared to the methods above, making use solely of surface structure with a uniform chemical coating or structuring an intrinsically hydrophobic material provide advantages such as chemical stability, robustness and precise wettability adjustment without the need for external disturbances, making it an ideal choice as microfluidic systems.

The distinctive advantage of microstructured surfaces lies on the precise adjustment of wettability *via* surface fabrication solely based on the morphological properties of the basic structure unit, such as micropillars or micro-striations. The motion of a liquid droplet sitting in the Cassie-Baxter (CB) state<sup>27</sup> on intrinsically hydrophobic microstructures with small hysteresis can be induced by a roughness gradient towards the region where its (effective) free surface energy is lower, once it has overcome hysteresis.<sup>21-23,26</sup> Additionally, external forces such as vibrations and coalescence have been exploited to overcome droplet adhesion and/or hysteresis in the presence of micropillars,<sup>23,24</sup> since otherwise the motion is limited.<sup>22</sup> However, spontaneous movement can be achieved on micro-striations with high length to width aspect ratio, for a much longer distance with only the help of the initial deposition energy and roughness gradient.<sup>21</sup> Further, micro-striated surfaces are expected to provide higher mobility and greater displacements along the striation direction<sup>28,29</sup> when compared to micropillared ones where the ratio of discontinuous segments of contact line length to surface area is greater.<sup>30-32</sup> Another relevant work is the long-range motion achieved via the combination of both roughness and chemical gradient in which only 6 micro-striated contrasts in series were considered.<sup>26</sup> We note here that after the first wettability contrast, inertial effect could not be decoupled from roughness and wetting gradients on the subsequent contrasting micro-striations. Hence, there is a lack of a unified criterion to describe the droplet displacement and velocity based solely on the structural parameters of the surface.

Despite the considerable focus on this area of research and the advancements reported in droplet motion so far, there is still a lack of understanding on how to precisely control the motion of a droplet using an array of a gradient of microstructures. Although it is well known that a greater intrinsic surface free energy difference would induce further displacements and higher velocities, given the existence of hysteresis and friction, the overall motion remains to be explained systematically. In the past, droplet motion on asymmetrical microstructures has been predicted by making use of simulations,<sup>33,34</sup> while other works have addressed a limited number of structural and wetting contrasts experimentally.<sup>22,23,26</sup> However, systematic experimental work exploring a wider range of wetting contrasts, *i.e.*, both average solid fraction and contrasting fraction, is necessary to develop a unified understanding of how motion of droplets can be controlled by surface structure. This is of paramount importance for the

formulation of the design guidelines for microfluidic devices and applications that need fine droplet control.

In this work, we have studied experimentally the dependence of droplet motion induced by a sharp structural gradient, paying special attention to the morphological properties of the surface microstructures/ micro-rails. We investigated the movement of a droplet over the boundary of two different micro-striated surfaces looking closely at the effect of structural parameters that may have an influence. Comparing to continuous gradients<sup>23</sup> or multiple structural units in series<sup>21,24,26</sup>, our contrasting striated surfaces provide a wide range of precise and pre-adjusted structural gradients, making it possible to systematically investigate the sole contribution of surface structure to the droplet motion. A criterion to predict the range of movement, henceforth referred to as displacement, and the motion speed is then put forward based on our experimental results. To acquire a further systematic knowledge of the motion, we additionally analysed experimentally the influence of inertial energy by releasing droplets from a controlled height as well as the influence of the droplet volume, on the displacement. This study contributes to understanding the mechanism of wettability-driven droplet motion, and proposes an instructive criterion when designing a surface microstructure for a specific displacement and velocity in microfluidic systems.

To study the correlation between surface structure and droplet motion, we fabricated micro-striated surfaces with pre-assigned height,  $h$ , width,  $w$ , and spacing,  $s$ , using photolithography and Deep Reactive-Ion Etching (Bosch process<sup>35</sup>) subsequently coated with a monolayer of perfluorodecyltrichlorosilane (FDTS), conferring homogeneous, intrinsic hydrophobicity to the micro-railed structures. Further surface fabrication details can be found in the accompanying Supplementary Information (SI). Fig. 1(a) shows Scanning Electron Microscopy (SEM) images of the straight boundary perpendicular to the contrasting striated surface. Solid fractions,  $\phi = w/(w + s)$  between 0.1 - 0.91, were achieved by varying  $s$  and  $w$  whilst  $h$  is kept constant and equals 20  $\mu\text{m}$ .

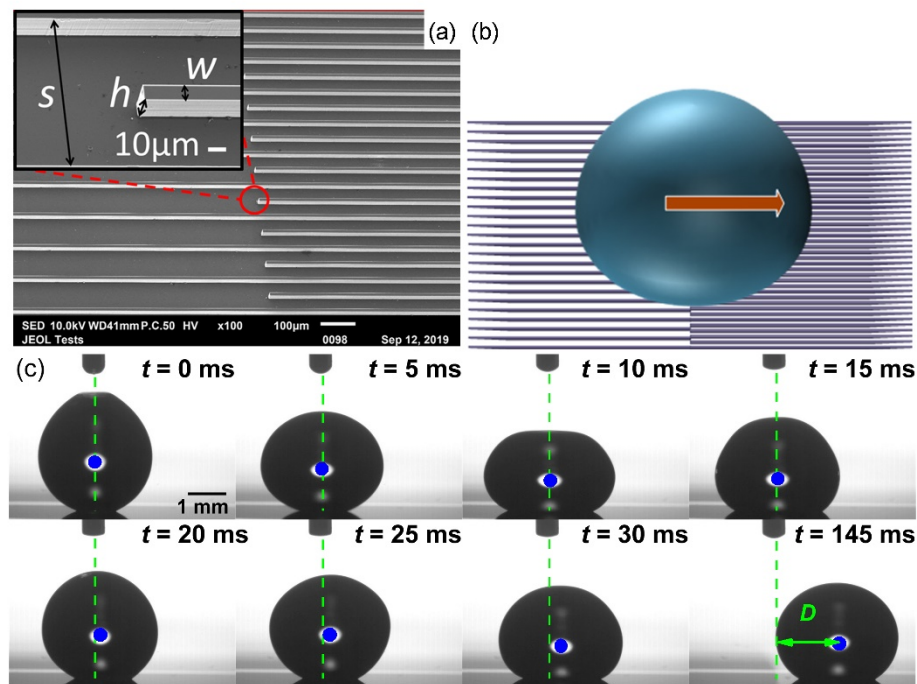


**FIG. 1 (a) SEM images of surface structure at the boundary of units 1 ( $\varphi = 0.10$ ) and 2 ( $\varphi = 0.20$ ). (b) Schematic diagram showing how droplet moves across the boundary. (c) Sequential photograph of a 9  $\mu\text{l}$  droplet moving on the boundary of unit 1 and unit 2. Part of the period of motion (5-30 ms) and the final position (145 ms) with displacement,  $D$ , of the centre of mass from the initial position to the instantaneous position, are presented. The blue dot represents the centre of mass of the droplet while the dashed line shows the position of the boundary on the surface, clearly visible in the last photo (145ms).**

Experimental observations of droplet motion on micro-striated surfaces with a contrast in surface structure were carried out by gentle deposition of a droplet of distilled water of volume  $V = 9 \mu\text{l}$  (with radius of *ca.* 1.3 mm, therefore being approximately spherical with characteristic length below  $\kappa^{-1}$ ) at the boundary between two different surface units, this latter was shown in Fig. 1(a). Droplet deposition was finely controlled by the dosing system of the Drop Shape Analyzer 100 (DSA 100, Krüss GmbH, Hamburg, Germany). Before droplet deposition, the visible contrasting striated boundary (due to the different light reflection as a consequence of the different structure solid fractions, see Fig. 1c at 145 ms) was manually positioned just beneath the droplet by making use of the x-y-z positioning system of the DSA 100. Unless otherwise specified, all the experiments were carried out under the same conditions. After the droplet detaches from the needle, it spreads on the surface and then moves towards the high solid fraction region. Given that the release height is approximately zero during gentle deposition, inertial effects due to droplet deposition/impingement can be neglected. The motion of the droplet was recorded with a high-speed camera (1000 fps) and then the position of the centre of mass was extracted with a custom-made MATLAB code. Fig. 1(c) shows an example of a droplet moving across the structural contrast.

Apparent, advancing and receding contact angles (CAs) for each structured surface unit as well as the intrinsic CA on the flat surface were measured using ADVANCE software from Krüss and are shown in Table I.

**TABLE I. Surface parameters  $w$ ,  $s$ , and**

8	20	5	0.80	114	2	$124 \pm 1$	106	1
9	50	5	0.91	110	1	$120 \pm 1$	103	3
Flat	\	\	\	111	1	$119 \pm 1$	105	3

Droplet motion is then induced by a contrast of solid fraction (in liquid contact) between two adjacent micro-striated surface units. Here, we present and discuss the influence of surface structure and the magnitude of the structural gradient on the droplet motion, *i.e.*, displacement and velocity. We found that both the difference of  $\varphi$  across the boundary, defined as  $\Delta\varphi = \varphi_R - \varphi_L$ , and the average value of  $\varphi$ , defined as  $\bar{\varphi} = (\varphi_R + \varphi_L)/2$ , have a strong direct impact on the motion, with subscript R and L define the right and left sides of the boundary.

We then plot the displacement,  $D$ , vs.  $\bar{\varphi}$  as shown in Fig. 2 where cases of  $D$  are distinguished based on different  $\Delta\varphi$ . For a given constant  $\Delta\varphi$ ,  $D$  has an (apparently) exponential decay with  $\bar{\varphi}$ , as the best fit. For solid units with larger  $\bar{\varphi}$  value, the droplet experiences a larger contact area with the surface inducing higher friction and greater CA hysteresis, eventually making the droplet less mobile. Besides, with an increase in  $\Delta\varphi$ , the trend of  $D$  shifts upwards.

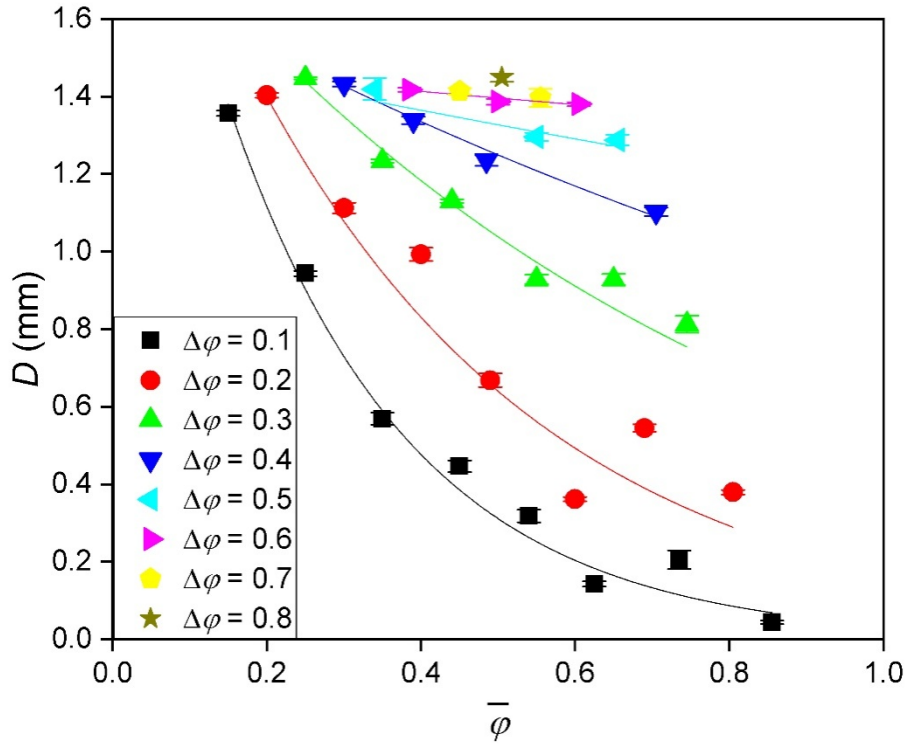


**FIG. 2. Displacement,  $D$  (mm), vs. average solid fraction,  $\bar{\varphi}$ , for different cases of contrasting solid fraction,  $\Delta\varphi$ . Exponential trends illustrate the best fit between displacement  $D$  and average solid fraction  $\bar{\varphi}$ . Each data point includes its associated standard error from 5 independent experiments.**

We now provide further analysis and discussion on the different parameters and forces present. On a (general) composite solid consisting of two different surface structures, fraction  $f_1$  having

an intrinsic contact angle of  $\theta_1$  and fraction  $f_2 = (1 - f_1)$ , an equivalent value of  $\theta_2$ , the effective contact angle,  $\theta^*$ , is given by the classic Cassie and Baxter equation:<sup>27</sup>

$$\cos \theta^* = f_1 \cos \theta_1 + (1 - f_1) \cos \theta_2. \quad (1)$$

If we then take  $f_1$  as the solid-liquid contact fraction,  $\varphi$ , with an intrinsic contact angle  $\theta_Y$ ,<sup>36</sup> and  $f_2$  represents air so that  $\cos \theta_2 = -1$ , the following relation is found:

$$\cos \theta^* = -1 + \varphi(\cos \theta_Y + 1), \quad (2)$$

By applying Eq. 2 to the expression for the initial driving force in the direction of motion for a 2-dimensional (2D) droplet, we get:

$$F_d = (\gamma_{SV} - \gamma_{SL})_R + (\gamma_{SL} - \gamma_{SV})_L = \gamma(\cos \theta_R^* - \cos \theta_L^*) = \gamma(\cos \theta_Y + 1)\Delta\varphi, \quad (3)$$

where  $\gamma_{SV}$  and  $\gamma_{SL}$  are the solid-vapor and solid-liquid surface tension and the subscripts R and L present the right and left edge of the 2D droplet. On the one hand, from Eq. 3, the initial driving force acting on the droplet,  $F_d$ , is dominated by the wettability gradient across the boundary. Then, for a fixed  $\bar{\varphi}$ , larger  $\Delta\varphi$  causes a greater driving force,  $F_d$ , and therefore, further droplet displacement, as clearly demonstrated in Fig. 2. On the other hand,  $\bar{\varphi}$  is an indicator of the surface area of the droplet in physical contact with the solid surface near the contact line, i.e., indicator of the resistance (friction). Hysteresis is also found to increase with increasing  $\varphi$  as shown in Table I.

From the two-dimensional (2D) force analysis above, it can be concluded that the motion displacement  $D$  is governed by two parameters;  $\bar{\varphi}$  and  $\Delta\varphi$ .  $\bar{\varphi}$  accounts for the resistance that prevents the droplet from moving  $F_r \propto \bar{\varphi}$  whilst  $\Delta\varphi$  represents the driving force exerted on the droplet  $F_d \propto \Delta\varphi$ . However, neither  $\bar{\varphi}$  nor  $\Delta\varphi$  alone can fully describe the motion. In order to depict these two forces acting on the droplet, we propose a unified criterion for the boundary, defined as:

$$\alpha = 2(\varphi_R - \varphi_L)/(\varphi_R + \varphi_L) = \Delta\varphi/\bar{\varphi}, \quad (4)$$

which can be regarded as the ratio of driving force to resistance. The results of  $D$  and average velocity,  $v$ , as functions of  $\alpha$  are shown in Fig. 3(a)&(b) respectively. The average velocity,  $v$ , is estimated as the displacement divided by elapsed time before the droplet stops.

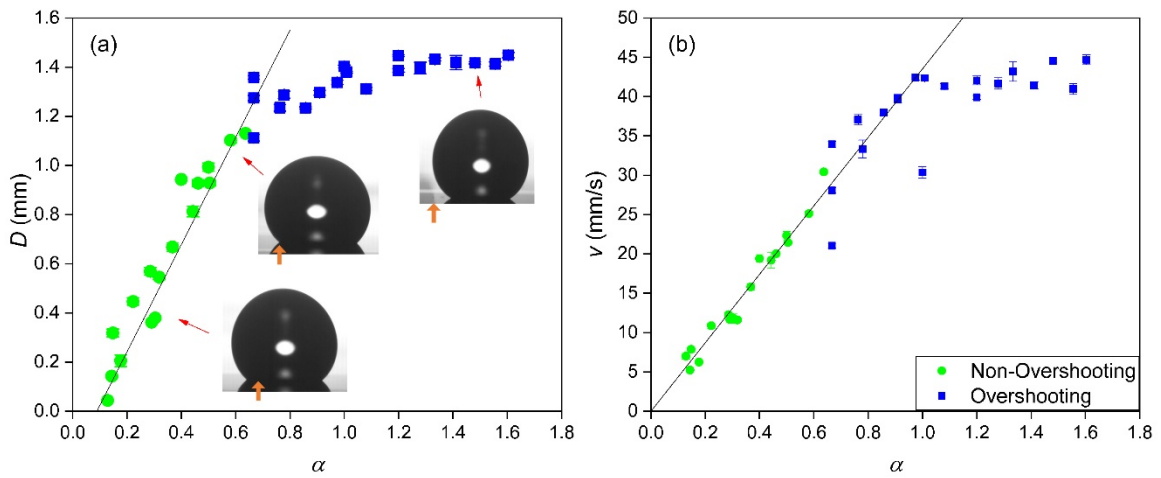


**FIG. 3. (a) Displacement,  $D$  (mm), and (b) average velocity,  $v$  (mm/s), vs. boundary criterion,  $\alpha$ . Green circles: Non-overshooting cases where the droplet eventually sits on the boundary. Blue squares: Overshooting cases where the droplet moves fully across the**

boundary. Each data point includes the standard error from five independent measurements. The coefficients of determination are 0.936 and 0.996 for the fitting lines for non-overshooting cases in (a) and (b) respectively.

In Fig. 3 (a), there is a clear trend shown by  $D$  vs.  $\alpha$ . Before  $\alpha$  reaches the threshold (of ca. 0.65), the droplet is unable to move entirely across the boundary due to the insufficiency of driving force combined with relatively high resistance. In these cases, results can be summarised by an empirical relation:  $D = 2.18(\alpha - 0.09)$  mm. 90% confidence intervals for the fitting coefficients of the prefactor ( $2.18 \pm 0.24$ ) and the intercept ( $0.09 \pm 0.02$ ) are found for  $\alpha$  between 0 and 0.65. The intercept indicates that, for a fixed intrinsic wettability of the surface structures, if the ratio of the driving force (provided by the contrasting structure across the boundary) to resistance force (from the liquid-solid contact area) is very small, no horizontal displacement occurs. The magnitude of this intercept represents resistance to the motion and will be a function of intrinsic surface hysteresis and friction to be overcome in order for the motion of the droplet to ensue. The prefactor is the slope obtained as linear fit of the data, which at the present remains as an empirical quantity accounting for other chemical and physical properties of the surface. With the increase of  $\alpha$ , the droplet is eventually able to move across the boundary completely and overshoots by a certain distance (blue squares). When the droplet overshoots with  $\alpha$  above 0.7,  $D$  deviates from the trend due to the lack of driving force after departure from the boundary and sits around 1.4 mm away from the boundary. With this relation, we can use the criterion  $\alpha$  to describe how far the droplet can move on the surface.

The average velocity,  $v$ , varies from ca. 5 mm/s to ca. 30 mm/s, which is also highly dependent on the geometrical properties across the boundary,  $\alpha$ , as shown in Fig. 3(b). We note here that the velocity calculation procedure by either averaging the velocity of the droplet before or after the droplet leaves the boundary did not provide any major qualitative or quantitative differences. A linear dependence of average velocity on  $\alpha$  is found at  $v = 44 \alpha$  mm/s. The fitting coefficient was found to be  $44 \pm 1$  with a 90% confidence interval. This relation is derived for the non-overshooting cases for  $\alpha$  between 0 and 0.65 in Fig. 3(b). However, it can be extrapolated up to  $\alpha = 1$  where the droplet overshoots not far from the boundary. For larger values of  $\alpha$ , the droplet velocity deviates from the trend due to the lack of driving force and becomes constant with values of ca. 30 mm/s, which is twice as fast as the micro-pillar cases.<sup>21</sup> By balancing the driving force  $F_d$ , viscous force  $F_v$  and contact line friction force  $F_{CL}$ , the droplet velocity takes the form:

$$v \cong \frac{\gamma(\cos\theta_Y + 1)}{2\xi} \frac{\Delta\phi}{\bar{\phi}}, \quad (5)$$

where  $\xi$  is a friction parameter accounting for the friction at the solid-liquid interface (see SI),  $\Delta\phi/\bar{\phi}$  equals  $\alpha$  and is only function of the structural properties, and  $\frac{\gamma(\cos\theta_Y + 1)}{2\xi}$  is proportional to the prefactor and function of the physical and chemical properties of the surface. Derivation of  $v$  can be found in the SI. It is clear that based on the geometrical criterion  $\alpha$  one can control the droplet velocity and displacement over a broad range of values with high accuracy, in particular the relative 90% confidence intervals are within 7% and 2% for the displacement,  $D$ , and the velocity,  $v$ , respectively.

To provide further insight into the actuation energy due to gravitational potential energy, we released droplets of volume,  $V$ , of 11  $\mu$ l (ca. 1.4 mm in radius and below  $\kappa^{-1}$ )

at different heights above the boundary of structural contrast on the surface correspond to different Weber



numbers,  $We$ , defined as  $We = \frac{2gH\rho R}{\gamma}$ , where  $H$  is the distance between the droplet bottom and the solid surface and  $R$ , the radius of an equivalent sphere with the same volume, is the characteristic length for the droplet:  $R = \left(\frac{3V}{4\pi}\right)^{\frac{1}{3}}$ . The regime of impingement studied here is far from that required to overcome the capillary pressure inducing the impalement of the droplets onto microstructures,<sup>37,38</sup>.  $D$  vs.  $We$  is shown in Fig. 4(a).

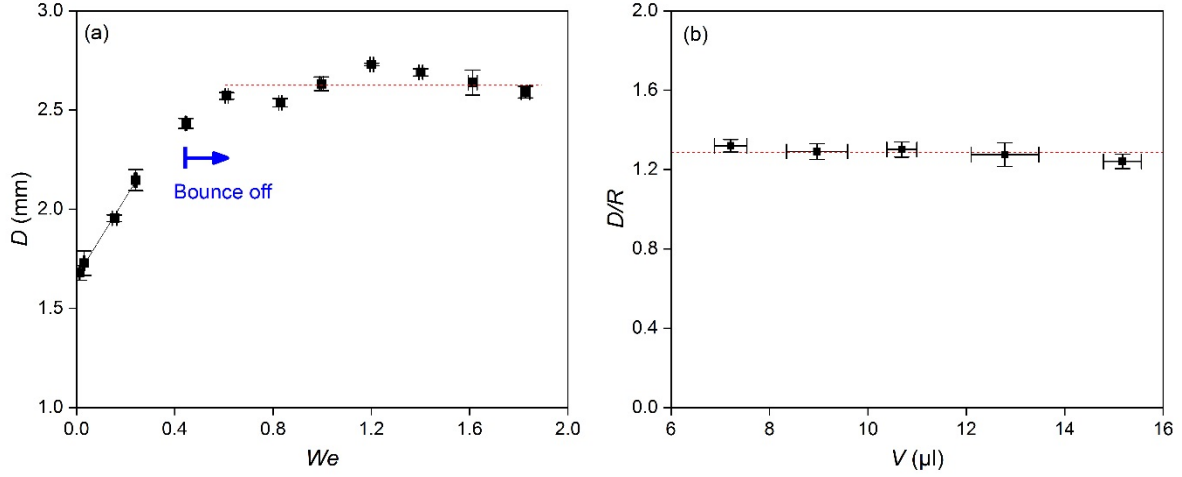


**FIG. 4. (a) Displacement,  $D$  (mm), vs. Weber number,  $We$ , at the boundary of structured units 1 ( $\varphi = 0.10$ ) and 2 ( $\varphi = 0.20$ ) with fixed  $\alpha = 0.67$ . The droplet bounces off the substrate when  $We$  is greater than *ca.* 0.4. (b) Displacement,  $D$  (mm), vs. droplet volume,  $V$  ( $\mu$ l), within the capillary length for water upon droplet gentle deposition, *i.e.*,  $We$  *ca.* 0, shown at the boundary of units 1 ( $\varphi = 0.10$ ) and 2 ( $\varphi = 0.20$ ), *i.e.*, fixed  $\alpha = 0.67$ . Error bars for each data point represent the standard error from 5 independent measurements. See SI for further analysis in the measurements and errors.**

It is found that  $D$  and the overshooting distance increase linearly with droplet release height,  $H$ , for  $We$  smaller than 0.4. For larger  $We$ , the droplet bounces off from the substrate after the first contact and then falls onto the substrate again without appreciable increase in  $D$  as inertial energy is increased further.

Finally, we address the effect of droplet size on the displacement upon gentle droplet deposition on the boundary, *i.e.*,  $H = 0$  and hence  $We = 0$ . In order to represent the displacement with respect to the different droplet sizes, we adopt  $D/R$  versus  $V$  in Fig. 4(b). The plateau trend indicates that there is no apparent change of  $D/R$  with increase in  $V$  between 7  $\mu$ l and 15  $\mu$ l (droplet radius below the capillary length). The size of the deposited droplet has hence little contribution to the movement.

We report here on the motion of a sessile droplet being deposited on the boundary of two micro-striated, surfaces varying in geometry, and therefore in the solid surface fraction presented to the liquid. We investigated the properties that influence the displacement and the velocity of the droplet motion. The influence of surface structure on the droplet motion was systematically studied for a wide range of solid fraction and contrasting fraction across the interface. A unified criterion, and  $\bar{\varphi}$  related to the driving and friction forces respectively) is proposed for the accurate prediction of the displacement and velocity of the droplet motion across a single boundary on micro-striated surfaces. Although the displacement is restricted without multiple contrast in sequence or a continuous gradient, this study is

fundamental and instructive for the optimization of several wettability contrast in series<sup>20,26</sup> permitting the droplet to reach specific location at certain velocities, of importance for specific engineering applications.

## Supplementary Material

See supplementary material for more information about the surface fabrication details, the interpretation of the velocity empirical relation and the experimental details.

## Acknowledgements

The authors would like to acknowledge the support of the European Space Agency through ESA Contract Number 4000129506/20/NL/PG, the support received from the Engineering and Physical Sciences Research Council (EPSRC) through the grant EP/P005705/1. The authors also acknowledge the EC-RISE-ThermaSMART project, which received funding from the European Union's Horizon 2020 research and innovation programme under the Marie Curie grant agreement No. 778104.

## Data Availability Statement

The data that supports the findings of this study are available within the article [and its supplementary material].

## References

- <sup>1</sup>R. Blossey, *Nature materials* **2**, 301 (2003).
- <sup>2</sup>S. Daniel, M. K. Chaudhury, and J. C. Chen, *Science* **291**, 633 (2001).
- <sup>3</sup>L. Cao, A. K. Jones, V. K. Sikka, J. Wu, and D. Gao, *Langmuir* **25**, 12444 (2009).
- <sup>4</sup>P. Zhang, Y. Maeda, F. Lv, Y. Takata, and D. Orejon, *ACS applied materials & interfaces* **9**, 35391 (2017).
- <sup>5</sup>Y. Zheng, H. Bai, Z. Huang, X. Tian, F. Q. Nie, Y. Zhao, J. Zhai, and L. Jiang, *Nature* **463**, 640 (2010).
- <sup>6</sup>O. D. Velev, B. G. Prevo, and K. H. Bhatt, *Nature* **426**, 515 (2003).
- <sup>7</sup>A. Wixforth, C. Strobl, C. Gauer, A. Toegl, J. Scriba, and Z. v. Guttenberg, *Analytical and bioanalytical chemistry* **379**, 982 (2004).
- <sup>8</sup>V. Srinivasan, V. K. Pamula, and R. B. Fair, *Lab on a Chip* **4**, 310 (2004).
- <sup>9</sup>F. De Angelis, F. Gentile, F. Mecarini, G. Das, M. Moretti, P. Candeloro, M. L. Coluccio, G. Cojoc, A. Accardo, C. Liberale *et al.*, *Nature Photonics* **5**, 682 (2011).
- <sup>10</sup>M. K. Chaudhury and G. M. Whitesides, *Science* **256**, 1539 (1992).
- <sup>11</sup>D. Orejon, O. Shardt, P. R. Waghmare, N. S. K. Gunda, Y. Takata, and S. K. Mitra, *RSC Advances* **6**, 36698 (2016).
- <sup>12</sup>O. Bliznyuk, J. R. Seddon, V. Veligura, E. S. Kooij, H. J. Zandvliet, and B. Poelsema, *ACS*

- 1 applied materials & interfaces **4**, 4141 (2012).
- 2 <sup>13</sup>O. Bliznyuk, H. P. Jansen, E. S. Kooij, H. J. Zandvliet, and B. Poelsema, Langmuir **27**, 11238  
3 (2011).
- 4 <sup>14</sup>B. Chandesris, U. Soupremanien, and N. Dunoyer, Colloids and Surfaces A: Physicochemical  
5 and Engineering Aspects **434**, 126 (2013).
- 6 <sup>15</sup>S. Daniel and M. K. Chaudhury, Langmuir **18**, 3404 (2002).
- 7 <sup>16</sup>J. Brzoska, F. Brochard-Wyart, and F. Rondelez, Langmuir **9**, 2220 (1993).
- 8 <sup>17</sup>K. Ichimura, S. K. Oh, and M. Nakagawa, Science **288**, 1624 (2000).
- 9 <sup>18</sup>J. S. Kuo, P. Spicar-Mihalic, I. Rodriguez, and D. T. Chiu, Langmuir **19**, 250 (2003).
- 10 <sup>19</sup>P. Y. Chiou, Z. Chang, and M. C. Wu, Journal of Microelectromechanical Systems **17**, 133  
11 (2008).
- 12 <sup>20</sup>D. Quéré, Annu. Rev. Mater. Res. **38**, 71 (2008).
- 13 <sup>21</sup>J. T. Yang, J. C. Chen, K. J. Huang, and J. A. Yeh, Journal of Microelectromechanical  
14 Systems **15**, 697 (2006).
- 15 <sup>22</sup>Y. Kita, C. M. Dover, A. Askounis, Y. Takata, and K. Sefiane, Soft matter **14**, 9418 (2018).
- 16 <sup>23</sup>A. Shastry, M. J. Case, and K. F. Böhringer, Langmuir **22**, 6161 (2006).
- 17 <sup>24</sup>C. Lv and P. Hao, Langmuir **28**, 16958 (2012).
- 18 <sup>25</sup>G. Fang, W. Li, X. Wang, and G. Qiao, Langmuir **24**, 11651 (2008).
- 19 <sup>26</sup>C. Liu, J. Sun, J. Li, C. Xiang, L. Che, Z. Wang, and X. Zhou, Scientific reports **7**, 7552  
20 (2017).
- 21 <sup>27</sup>A. Cassie and S. Baxter, Transactions of the Faraday society **40**, 546 (1944).
- 22 <sup>28</sup>Z. Yoshimitsu, A. Nakajima, T. Watanabe, and K. Hashimoto, Langmuir **18**, 5818 (2002).
- 23 <sup>29</sup>M. Kumar, R. Bhardwaj, and K. C. Sahu, Langmuir **35**, 2957 (2019).
- 24 <sup>30</sup>W. Xu and C. H. Choi, Physical review letters **109**, 024504 (2012).
- 25 <sup>31</sup>A. T. Paxson and K. K. Varanasi, Nature communications **4**, 1492 (2013).
- 26 <sup>32</sup>F. Schellenberger, N. Encinas, D. Vollmer, and H. J. Butt, Physical review letters **116**,  
27 096101 (2016).
- 28 <sup>33</sup>G. Tang, H. Xia, and Y. Shi, Journal of Applied Physics **117**, 244902 (2015).
- 29 <sup>34</sup>N. Moradi, F. Varnik, and I. Steinbach, EPL (Europhysics Letters) **89**, 26006 (2010).
- 30 <sup>35</sup>F. Laermer and A. Schilp, (Google Patents, 1996).
- 31 <sup>36</sup>T. Young, Philosophical transactions of the royal society of London, 65 (1805).
- 32 <sup>37</sup>D. Bartolo, F. Bouamrine, E. Verneuil, A. Buguin, P. Silberzan, and S. Moulinet, EPL  
33 (Europhysics Letters) **74**, 299 (2006).
- 34 <sup>38</sup>Y. C. Jung and B. Bhushan, Langmuir **24**, 6262 (2008).

## Supporting Information

### Droplet Motion on Contrasting Striated Surfaces

Hongyu Zhao <sup>a</sup>, Daniel Orejon<sup>a</sup>, Coinneach Mackenzie-Dover <sup>b</sup>, Prashant Valluri <sup>a</sup>, Martin E.R. Shanahan<sup>c</sup> and Khellil Sefiane<sup>a,d\*</sup>

<sup>a</sup>Institute for Multiscale Thermofluids, School of Engineering, The University of Edinburgh, EH9 3FD, Scotland, UK

<sup>b</sup>Oden Institute for Computational Engineering and Sciences, The University of Texas at Austin, Texas TX 78712, USA

<sup>c</sup>University of Bordeaux, I2M, UMR 5295, F-33400 Talence, France

<sup>d</sup>Tianjin Key Lab of Refrigeration Technology, Tianjin University of Commerce, Tianjin City 300134, China

#### Abstract

Liquid droplets move readily under the influence of surface tension gradients on their substrates. Substrates decorated with parallel microgrooves, or striations, presenting the advantage of homogeneous chemical properties yet varying the topological characteristics on either side of a straight-line boundary are considered in this study. The basic type of geometry consists of hydrophobic micro-striations/rails perpendicular to the boundary, with the systematic variation of the width to spacing ratio, thus changing the solid-liquid contact fraction and inducing a well-defined wettability contrast across the boundary. Droplets in the Cassie-Baxter state, straddling the boundary, move along the wettability contrast in order to reduce the overall surface free energy. Results show the importance of average solid fraction and contrasting fraction in a wide range for given geometries across the boundary on droplet motion. A unified criterion for contrasting striated surfaces, which successfully describes the displacement and the velocity of the droplets, is suggested, providing guidelines for droplet manipulation on micro-striated/railed surfaces.

\*Authors to whom correspondence should be addressed.

Electronic mail: Khellil Sefiane: [k.sefiane@ed.ac.uk](mailto:k.sefiane@ed.ac.uk)

## Details on surface fabrication

4-inch silicon wafer were purchased from Si-Mat (Silicon Materials, Landsberg, Germany). Thereafter, hexamethyldisilazane (HMDS) was applied to the wafer as adhesive for the photoresist for 10 minutes. We note here that no further cleaning procedure was carried out as any further cleaning or wet cleaning treatment may indeed induced further deposition of dirt or contaminants. Then, wafers were placed in an SVG 8600 (Silicon Valley Group, USA) track system in order to dispense and spin coat a SPR 350 photoresist layer of 1.2  $\mu\text{m}$  in thickness. Then, the wafer and the photoresist are soft-baked on a heating plate at 90  $^{\circ}\text{C}$  for 60s, exposed for 5 seconds in vacuum inside a Karl Suss MA8 mask aligner (Süss, Garching, Germany) and further developed inside the SVG 8600. The substrates were then covered by a pre-designed mask displaying the desired micro-structure patterns, which were then exposed to UV light through the mask. After the development process, the exposed resist was washed away, leaving the patterned resist on the substrates.

The substrates were then subjected deep reactive-ion etching (deep RIE, Bosch process) in a surface technology system STS Multiplex ICP (inductively coupled plasma) etching for 20 cycles. After etching, the resist was removed from the substrate by acetone, leaving the rigid microstructures with a height of 20  $\mu\text{m}$  on the substrates.

The surface fabrication was carried out within the Class 10 cleanrooms of the Scottish Microelectronic Centre (SMC). After fabrication, the substrates were sealed in a wafer box and sent to Memstar Ltd., Scotland for coating. A monolayer of Perfluorodecyltrichlorosilane (FDTS) was applied onto the substrates, making the surface microstructures intrinsically hydrophobic.

## Interpretation of the prefactor for the expression of velocity

On one hand, for the resistance forces in the direction of motion for a two-dimensional (2D) droplet with a unit thickness, firstly we consider the viscous force  $F_v$ :

$$F_v = \int \mu \frac{\partial v_x}{\partial y} dS_b \cong \mu \frac{v}{r} \cdot 2r\bar{\varphi} = 2\mu\bar{\varphi}v, \quad (\text{SI.1})$$

where  $v_x$  is the velocity in droplet bulk,  $v$  is the droplet velocity,  $S_b = 2r\bar{\varphi}$  is the base solid-liquid contact area,  $\mu$  is the liquid viscosity,  $\bar{\varphi}$  is the average solid fraction between 2 wettability contrast units, and  $r$  is the droplet base radius in contact with the structured surface. In addition, the friction at the three-phase contact line (CL)  $F_{\text{CL}}$ , which typically governs the resistance force on structured surfaces, is expressed as follows:

$$F_{\text{CL}} = 2\xi\bar{\varphi}v, \quad (\text{SI.2})$$

where  $\xi$  is the friction parameter accounting for the friction at the solid-liquid interface.

The driving force  $F_d$  is on the other hand expressed as in Eq. 3 of the main manuscript:

$$F_d = (\gamma_{SV} - \gamma_{SL})_R + (\gamma_{SL} - \gamma_{SV})_L = \gamma(\cos \theta_R^* - \cos \theta_L^*) = \gamma(\cos \theta_Y + 1)\Delta\phi \quad (\text{SI.3})$$

Then, balancing the driving force (Eq. SI.3), viscous force (Eq. SI.1), and contact line force (Eq. SI.2), we derive an expression for the velocity  $v$  as Eq. SI.4:

$$v \cong \frac{\gamma(\cos \theta_Y + 1)\Delta\phi}{2(\xi + \mu)\bar{\phi}} = \frac{\gamma(\cos \theta_Y + 1)}{2(\xi + \mu)}\alpha. \quad (\text{SI.4})$$

Given  $\gamma \cong 7.2 \cdot 10^{-2} \text{ N/m}$ ,  $\mu = 8.9 \cdot 10^{-4} \text{ Pa} \cdot \text{s}$ ,  $(\cos \theta_Y + 1) \cong 0.66$ ,  $r \cong 10^{-3} \text{ m}$ , and the empirical equation:  $v = 34 \alpha \text{ mm/s}$ , we can estimate the contact line friction parameter as  $\xi \cong 0.7 \text{ Pa} \cdot \text{s}$ . Then, for  $\xi \gg \mu$  contact line friction dominates the resistance against droplet motion and Eq. SI.4 can be simplified as Eq. SI.5 (Eq. 5 of the main manuscript):

$$v \cong \frac{\gamma(\cos \theta_Y + 1)}{2\xi}\alpha. \quad (\text{SI.5})$$

In Eq. SI.5 and Eq. 5 of the main manuscript,  $\alpha$  is solely function of the structural properties between two units, while  $\frac{\gamma(\cos \theta_Y + 1)}{2\xi}$  is in turn solely function of the chemical properties of the surface and the fluid, *i.e.*, surface tension liquid-gas and intrinsic wettability of the surface. Then it seems reasonable to group  $\frac{\gamma(\cos \theta_Y + 1)}{2\xi}$  within the proposed prefactor.

## Measurement error for droplet volume

The error bar for volume in Fig 4(b) is the standard error from 5 independent measurements and calculations via image processing. The deviation of volume comes from the difficulty to deposit water droplet onto hydrophobic surfaces with low solid fraction, *i.e.*, superhydrophobic surfaces. When the volume is small, it is difficult for the water droplet to detach from the needle due to the low adhesion between the droplet and the hydrophobic surface, and when the volume is large, the surface tension cannot always hold the dosed droplet as a whole, leaving a small part of droplet attached to the needle, hence dosing less volume than expected.